Verifying Provable Stability Domains for Discrete-Time Systems Using Ellipsoidal State Enclosures

Andreas Rauh, Auguste Bourgois, Luc Jaulin

▶ **To cite this version:**

Andreas Rauh, Auguste Bourgois, Luc Jaulin. Verifying Provable Stability Domains for Discrete-Time Systems Using Ellipsoidal State Enclosures. Acta Cybernetica, 2023, 26 (2), pp.267-291. 10.14232/actacyb.293871 . hal-03670858

HAL Id: hal-03670858

https://ensta-bretagne.hal.science/hal-03670858

Submitted on 17 May 2022

HAL is a multi-disciplinary open access archive for the deposit and dissemination of scientific research documents, whether they are published or not. The documents may come from teaching and research institutions in France or abroad, or from public or private research centers.

L'archive ouverte pluridisciplinaire **HAL**, est destinée au dépôt et à la diffusion de documents scientifiques de niveau recherche, publiés ou non, émanant des établissements d'enseignement et de recherche français ou étrangers, des laboratoires publics ou privés.

Acta Cybernetica — *online–first paper version* — pages 1–25.

Verifying Provable Stability Domains for Discrete-Time Systems Using Ellipsoidal State Enclosures

Andreas Rauh[a], Auguste Bourgois[bcd], and Luc Jaulin[de]

Abstract

Stability contractors, based on interval analysis, were introduced in recent work as a tool to verify stability domains for nonlinear dynamic systems. These contractors rely on the property that — in case of provable asymptotic stability — a finitely large domain in a multi-dimensional state space is mapped into its interior after a certain integration time for continuous-time processes or after a certain number of discretization steps in a discrete-time setting. However, a disadvantage of the use of axis-aligned interval boxes in such computations is the omnipresent wrapping effect. As shown in this contribution, the replacement of classical interval representations by ellipsoidal domain enclosures reduces this undesirable effect. It also helps to find suitable ratios for the edge lengths if interval-based domain representations are investigated. Moreover, ellipsoidal domains naturally represent the possible regions of attraction of asymptotically stable equilibrium points that can be analyzed with the help of quadratic Lyapunov functions, for which stability criteria can be cast into linear matrix inequality (LMI) constraints. For that reason, this paper further presents possible interfaces of ellipsoidal enclosure techniques with LMI approaches. This combination aims at the maximization of those domains that can be proven to be stable for a discrete-time range-only localization algorithm in robotics. There, an Extended Kalman Filter (EKF) is applied to a system for which the dynamics are characterized by a discrete-time integrator disturbance model with additive Gaussian noise. In this scenario, the measurement equations correspond to the distances between the object to be localized and beacons with known positions.

Keywords: stability analysis, ellipsoidal enclosures, interval methods, Kalman filtering

[a]Carl von Ossietzky Universität Oldenburg, Department of Computing Science, Group: Distributed Control in Interconnected Systems, D-26111 Oldenburg, Germany, E-mail: Andreas.Rauh@uni-oldenburg.de, ORCID: 0000-0002-1548-6547

[b]FORSSEA, Paris, France

[c]E-mail: Auguste.Bourgois@ensta-bretagne.org, ORCID: 0000-0002-0333-5872

[d]ENSTA Bretagne, Lab-STICC, 29806 Brest, France

[e]E-mail: lucjaulin@gmail.com, ORCID: 0000-0002-0938-0615

DOI: 10.14232/actacyb.293871

1 Introduction

The analysis of stability properties of nonlinear dynamic systems is a crucial aspect for the verification of control and state estimation procedures (i.e., state observers) in many different areas. From a methodological point of view, Lyapunov function techniques can be applied to deal with this task for both discrete-time and continuous-time processes [18, 19]. They are not only applicable to the analysis of predefined control and observer structures but are also widely used during their synthesis. Especially when system models with a linear or quasi-linear structure are considered, there exist a large number of interrelations between Lyapunov function techniques and LMIs. This is basically caused by the fact that stability criteria for linear dynamic systems, which are investigated with the help of quadratic candidates for Lyapunov functions, are equivalent to criteria that can be stated with the help of LMIs.

Based on these fundamental observations, numerous research activities have been performed in recent years which (as an obviously non-exhaustive list) deal with the following aspects:

- transforming stability requirements for linear uncertain system models with polytopic time-invariant and time-varying uncertainty into sets of LMIs [2, 5, 8, 9, 40];
- development of iterative LMI techniques for synthesizing robust output and state feedback controllers for systems which are simultaneously subject to polytopic parameter uncertainty and/or stochastic noise [11, 28, 32, 41];
- verifying invariant sets of nonlinear closed-loop control systems [37];
- implementing gain scheduling controllers for quasi-linear systems with bounded parameter uncertainty [17];
- implementing online gain adaptation schemes for variable-structure, sliding mode controllers as well as backstepping techniques with the aim of chattering reduction [33–35];
- investigation of the dual task of variable-structure state estimation [31];
- finding optimal candidates for Lyapunov functions for nonlinear dynamic systems [22, 43];
- determining the region of attraction of stable operating points and maximizing the provable stability domains for nonlinear processes [7, 12, 15, 25, 44–46].

In parallel to the development of the above-mentioned Lyapunov and LMI techniques, interval methods have been investigated during the last decades [16,20]. Due to their fundamental property to enclose the solution to some mathematically formulated problem in a guaranteed way, they have many applications in engineering. These cover aspects such as state and parameter estimation [1], uncertainty quantification in robotics applications [21, 24], or simulation of dynamic systems [23].

Moreover, a new technique for enclosing provable stability domains was presented recently in [3, 4]. This so-called stability contractor is re-investigated in this paper for analyzing stability properties of a discrete-time EKF [42] that is applied to the task of localizing a robot with the help of range-only measurements. For that purpose, the interval-based implementation of this contractor is compared with a novel ellipsoidal enclosure approach. This approach was recently presented in [29, 30] as a tool for nonlinear function evaluation, simulation of dynamic system models, as well as performance analysis of linearization-based stochastic filters (such as the EKF). In [26], it has been extended towards a state estimation procedure which exploits a quasi-linear system structure when determining inner and outer bounds for state enclosures.

This paper is structured as follows: Sec. 2 summarizes the already existing interval-based stability contractor and reviews ellipsoidal enclosure techniques for discrete-time dynamic systems. Both provide the basis for the novel ellipsoidal stability contractor in Sec. 3 which enhances the original interval-based technique due to its capability for often proving larger regions of attraction for stable operating points. A (near to optimal) parameterization of this novel contractor is described in Secs. 3.1 and 3.2 with an illustrating example in Sec. 3.3 and its use for a localization task in robotics in Sec. 3.4. Moreover, a new extension for proving instability of equilibrium points is presented in Sec. 3.5. Finally, Sec. 4 describes an outlook on using ellipsoidal techniques for finding positive invariant domains in the frame of continuous-time processes before conclusions are given in Sec. 5.

2 Preliminaries

In this section, fundamental preliminaries published in previous works of the authors are given. These are the interval-based stability contractor [3, 4] as well as (thick) ellipsoidal state enclosure techniques for discrete-time systems. For the latter, we make a distinction between a general formulation [29, 30] and a specialized version for quasi-linear system models [26].

2.1 Notation

Throughout this paper, scalar interval variables with the lower and upper bounds $\underline{x}$ and $\overline{x}$, respectively, where $\underline{x} \leq \overline{x}$, are denoted as $[x] = [\underline{x}\ ;\ \overline{x}]$. For the vector-valued case, an interval vector (also called *interval box*) is formed as the Cartesian product of scalar intervals according to the stacked notation

$$[\mathbf{x}] = \begin{bmatrix} [x_1] & \dots & [x_n] \end{bmatrix}^T \quad , \tag{1}$$

where the set of axis-aligned interval boxes in $\mathbb{R}^n$ is denoted as $\mathbb{IR}^n$. For fundamental enclosure properties of interval analysis as well as interval extensions of (vector-valued) functions $\mathbf{f} : \mathbb{R}^m \mapsto \mathbb{R}^n$, the reader is referred to [16, 20].

Moreover, according to [29,30], define a thick ellipsoid $(\!(\mathscr{E})\!) = (\!(\mathscr{E})\!)\left(\boldsymbol{\mu}, \boldsymbol{\Gamma}, \left[\underline{\rho}\,;\,\overline{\rho}\right]\right)$, where $0 \leq \underline{\rho} \leq \overline{\rho}$, as a subset of the power set $\mathscr{P}(\mathbb{R}^n)$ so that

$$(\!(\mathscr{E})\!) = \left\{ \mathscr{A} \in \mathscr{P}(\mathbb{R}^n) \;\middle|\; \mathscr{E}^{\mathrm{I}} \subseteq \mathscr{A} \subseteq \mathscr{E}^{\mathrm{O}} \right\} \tag{2}$$

encloses a set $\mathscr{A}$ of interest both from the inside and outside with the inner and outer bounding ellipsoids

$$\begin{aligned} \mathscr{E}^{\mathrm{I}} &= \left\{ \mathbf{x} \in \mathbb{R}^n \;\middle|\; (\mathbf{x}-\boldsymbol{\mu})^T \left(\underline{\rho}\boldsymbol{\Gamma}\right)^{-T} \left(\underline{\rho}\boldsymbol{\Gamma}\right)^{-1} (\mathbf{x}-\boldsymbol{\mu}) \leq 1 \right\} \;\;, \\ \mathscr{E}^{\mathrm{O}} &= \left\{ \mathbf{x} \in \mathbb{R}^n \;\middle|\; (\mathbf{x}-\boldsymbol{\mu})^T \left(\overline{\rho}\boldsymbol{\Gamma}\right)^{-T} \left(\overline{\rho}\boldsymbol{\Gamma}\right)^{-1} (\mathbf{x}-\boldsymbol{\mu}) \leq 1 \right\} \end{aligned} \tag{3}$$

that have surfaces parallel to each other.

Finally, $\|\cdot\|$ represents (an interval extension of) the Euclidean norm of the corresponding vector-valued argument as introduced in [29]; the relations $\mathbf{M} \succ 0$ and $\mathbf{M} \succeq 0$ denote positive and positive semi-definiteness of a real-valued symmetric matrix ($\mathbf{M} \prec 0$ and $\mathbf{M} \preceq 0$, negative (semi-) definiteness, respectively).

2.2 Interval-Based Stability Contractors

Consider an interval box $[\mathbf{x}_0]$ of $\mathbb{R}^n$. According to [4, Def. 1], a stability contractor $\Psi : \mathbb{IR}^n \mapsto \mathbb{IR}^n$ of rate $|\alpha| < 1$ is characterized by the following properties for all boxes $[\mathbf{a}], [\mathbf{b}] \subset [\mathbf{x}_0]$:

1. monotonicity: $[\mathbf{a}] \subset [\mathbf{b}] \Longrightarrow \Psi\left([\mathbf{a}]\right) \subset \Psi\left([\mathbf{b}]\right)$;
2. contractance: $\Psi\left([\mathbf{a}]\right) \subset [\mathbf{a}]$;
3. equilibrium: $\Psi(\mathbf{0}) = \mathbf{0}$;
4. convergence: $\Psi\left([\mathbf{a}]\right) \subset \alpha \cdot [\mathbf{a}] \Longrightarrow \forall k \geq 1, \Psi^k\left([\mathbf{a}]\right) \subset \alpha^k \cdot [\mathbf{a}]$, where $\Psi^k\left([\mathbf{a}]\right)$ denotes the iterated evaluation $\underbrace{\Psi \circ \ldots \circ \Psi}_{k}$, where Ψ^0 is the identity function.

As shown in [4], the existence of such a stability contractor with $\Psi\left([\mathbf{x}_0]\right) \subset [\mathbf{x}_0]$ can serve as a proof of Lyapunov stability of a discrete-time dynamic system

$$\mathbf{x}_{k+1} = \mathbf{f}(\mathbf{x}_k) \;\;, \quad \mathbf{f} : \mathbb{R}^n \mapsto \mathbb{R}^n \tag{4}$$

with the equilibrium state $\mathbf{x} = \mathbf{0}$, i.e., $\mathbf{0} = \mathbf{f}(\mathbf{0})$ in the complete box of initial conditions $[\mathbf{x}_0] \ni \mathbf{0}$.

Remark 1. Due to the fact that a centered form representation of the interval extension of functions such as the system model (4) often leads to tighter bounds of the resulting state enclosures than a naive interval extension if the domain on which the function is evaluated is sufficiently small (cf. [10]), an evaluation of the

stability contractor in centered form representation was proposed in [4]. Moreover, it should be noted that a one-step evaluation of the state equations (especially for systems with oscillatory but asymptotically stable dynamics), often does not satisfy the contractance property mentioned above. Then, the stability contractor can be applied to a multi-time step evaluation by using a k times iterated centered form representation of (4) on the box of initial conditions.

2.3 Ellipsoidal Enclosures for Discrete-Time Dynamic Systems: General Case

Consider a finite-dimensional discrete-time system model (4), where (as also required for the centered form representation in the previous subsection) $\mathbf{f}$ is assumed to be differentiable. Given a thick ellipsoid representation

$$\left(\!\!\left(\mathscr{E}\right)\!\!\right)_k = \left(\!\!\left(\mathscr{E}\right)\!\!\right)\left(\boldsymbol{\mu}_k, \boldsymbol{\Gamma}_k, \left[\underline{\rho}_k \,;\, \overline{\rho}_k\right]\right) \tag{5}$$

at the time instant k, a thick ellipsoid

$$\left(\!\!\left(\mathscr{E}\right)\!\!\right)_{k+1} = \left(\!\!\left(\mathscr{E}\right)\!\!\right)\left(\boldsymbol{\mu}_{k+1}, \boldsymbol{\Gamma}_{k+1}, \left[\underline{\rho}_{k+1} \,;\, \overline{\rho}_{k+1}\right]\right) \tag{6}$$

at the instant $k+1$ is defined by the following Theorem 1 such that $\mathscr{E}^{\mathrm{I}}_{k+1}$ is an inner boundary containing certainly reachable states and $\mathscr{E}^{\mathrm{O}}_{k+1}$ is a guaranteed outer enclosure. A graphical representation of this enclosure property is given in Fig. 1. For a proof of the following theorem, the reader is referred to [30].

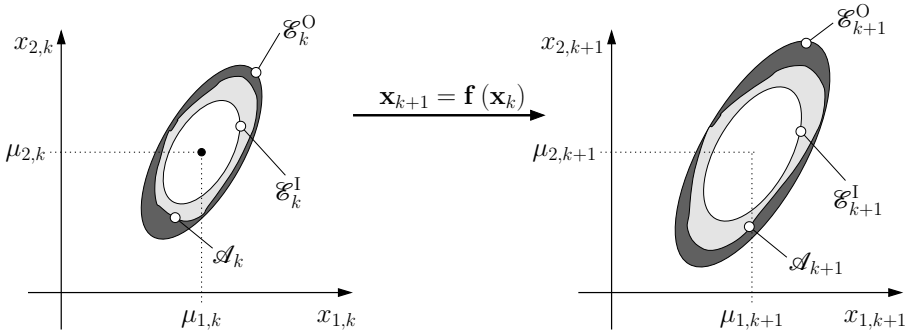

Figure 1: Definition of a thick ellipsoid $\left(\!\!\left(\mathscr{E}\right)\!\!\right)_k$ enclosing the domain $\mathscr{A}_k$ and its mapping $\left(\!\!\left(\mathscr{E}\right)\!\!\right)_{k+1}$ via the system model (4) that encloses the true solution set $\mathscr{A}_{k+1}$ from the inside and outside.

Theorem 1 ([29,30] Thick ellipsoid enclosures)**.** *Define the state enclosure at the time instant k by the thick ellipsoid $\left(\!\!\left(\mathscr{E}\right)\!\!\right)_k$. For a differentiable state equation (4), with*

$$\mathbf{A}_k = \frac{\partial \mathbf{f}}{\partial \mathbf{x}_k}\left(\boldsymbol{\mu}_k\right) \quad \textit{invertible} \ , \tag{7}$$

$\left(\!\left(\mathscr{E}\right)\!\right)_{k+1}$ *according to (6) is a thick ellipsoid enclosure of the solution set* $\mathbf{f}\left(\left(\!\left(\mathscr{E}\right)\!\right)_k\right)$ *with*

$$\boldsymbol{\mu}_{k+1} = \mathbf{f}\left(\boldsymbol{\mu}_k\right) \quad \textit{and} \quad \boldsymbol{\Gamma}_{k+1} = \mathbf{A}_k \cdot \boldsymbol{\Gamma}_k \tag{8}$$

as well as

$$\underline{\rho}_{k+1} = (1 - \rho_{\mathrm{I},k}) \cdot \underline{\rho}_k \quad \textit{and} \quad \overline{\rho}_{k+1} = (1 + \rho_{\mathrm{O},k}) \cdot \overline{\rho}_k \ . \tag{9}$$

Here,

$$\rho_{\mathrm{I},k} = \max_{\|\tilde{\mathbf{x}}_k\| \leq 1} \left\| \tilde{\mathbf{b}}_{\mathrm{I},k}\left(\tilde{\mathbf{x}}_k\right) \right\| \ , \tag{10}$$

$$\tilde{\mathbf{b}}_{\mathrm{I},k}\left(\tilde{\mathbf{x}}_k\right) = \underline{\rho}_k^{-1} \boldsymbol{\Gamma}_k^{-1} \mathbf{A}_k^{-1} \cdot \left(\mathbf{f}\left(\underline{\rho}_k \boldsymbol{\Gamma}_k \tilde{\mathbf{x}}_k + \boldsymbol{\mu}_k \right) - \mathbf{f}\left(\boldsymbol{\mu}_k\right) \right) - \tilde{\mathbf{x}}_k \tag{11}$$

and

$$\rho_{\mathrm{O},k} = \max_{\|\tilde{\mathbf{x}}_k\| \leq 1} \left\| \tilde{\mathbf{b}}_{\mathrm{O},k}\left(\tilde{\mathbf{x}}_k\right) \right\| \ , \tag{12}$$

$$\tilde{\mathbf{b}}_{\mathrm{O},k}\left(\tilde{\mathbf{x}}_k\right) = \overline{\rho}_k^{-1} \boldsymbol{\Gamma}_k^{-1} \mathbf{A}_k^{-1} \cdot \left(\mathbf{f}\left(\overline{\rho}_k \boldsymbol{\Gamma}_k \tilde{\mathbf{x}}_k + \boldsymbol{\mu}_k \right) - \mathbf{f}\left(\boldsymbol{\mu}_k\right) \right) - \tilde{\mathbf{x}}_k \, . \tag{13}$$

2.4 Ellipsoidal Enclosures for Discrete-Time Dynamic Systems: Quasi-Linear Case

As a special case of the general system model (4), consider the quasi-linear system representation

$$\mathbf{x}_{k+1} = \mathbf{A}\left(\mathbf{x}_k, \mathbf{p}_k\right) \cdot \mathbf{x}_k \ , \tag{14}$$

where $\mathbf{A}\left(\mathbf{x}_k, \mathbf{p}_k\right) \in \mathbb{R}^{n \times n}$ is a state- and parameter-dependent system matrix. This matrix can be extracted from the general system formulation (4) either by means of factoring out the state vector in such a way that all matrix entries are finite and non-singular in the operating domain of interest. Alternatively, it can be bounded by means of slope calculus [6] or in analogy to the centered form representation mentioned before by means of an interval extension of the system's Jacobian, see also [26].

Remark 2. To prove asymptotic stability by means of the contractor technique in Sec. 2.2, it is necessary that the matrix $\mathbf{A}\left(\mathbf{x}_k, \mathbf{p}_k\right)$ in (14) does not introduce any further equilibrium point (except for the origin of the state space) in the evaluation domain of interest. This is a direct consequence of the contractance property in Sec. 2.2 which must equally hold for the state equations if the interval-based stability contractor of Sec. 2.2 and the general ellipsoidal evaluation technique of Sec. 2.3 were applied.

The following five-step evaluation procedure for quasi-linear discrete-time systems (14) was published as a state prediction algorithm in the frame of a predictor–corrector state estimator in [26]. As visualized in Fig. 2, this procedure is based on propagating a thick ellipsoid $\left(\!\left(\check{\mathscr{E}}\right)\!\right)_k$ centered at the origin of the state space in parallel to an offset term (arising from non-zero ellipsoid midpoints $\boldsymbol{\mu}_k$) in the form

$$\mathbf{x}_{k+1} = \mathbf{A}\left(\mathbf{x}_k, \mathbf{p}_k\right) \cdot \check{\mathbf{x}}_k + \tilde{\mathbf{A}}_k \cdot \boldsymbol{\mu}_k + \left(\mathbf{A}\left(\mathbf{x}_k, \mathbf{p}_k\right) - \tilde{\mathbf{A}}_k \right) \cdot \boldsymbol{\mu}_k \, , \tag{15}$$

where

$$\left(\!\left(\mathscr{E}\right)\!\right)_k = \left(\!\left(\mathscr{E}\right)\!\right)_k \left(\boldsymbol{\mu}_k, \boldsymbol{\Gamma}_k, \left[\underline{\rho}_k \; ; \; \overline{\rho}_k\right]\right) \tag{16}$$

denotes the uncertainty on the non-origin centered states $\mathbf{x}_k$,

$$\left(\!\left(\check{\mathscr{E}}\right)\!\right)_k = \left(\!\left(\check{\mathscr{E}}\right)\!\right)_k \left(\mathbf{0}, \boldsymbol{\Gamma}_k, \left[\underline{\rho}_k \; ; \; \overline{\rho}_k\right]\right) \tag{17}$$

the uncertainty of $\check{\mathbf{x}}_k$ after shifting the ellipsoid to the origin, and

$$\tilde{\mathbf{A}}_k = \mathbf{A}\left(\boldsymbol{\mu}_k, \operatorname{mid}\left([\mathbf{p}_k]\right)\right) \tag{18}$$

the midpoint approximation of the quasi-linear system matrix with

$$\mathbf{p}_k \in [\mathbf{p}_k] = \left[\underline{\mathbf{p}}_k \; ; \; \overline{\mathbf{p}}_k\right] \;, \quad \text{where} \quad \operatorname{mid}\left([\mathbf{p}_k]\right) = \frac{1}{2} \cdot \left(\underline{\mathbf{p}}_k + \overline{\mathbf{p}}_k\right) \;. \tag{19}$$

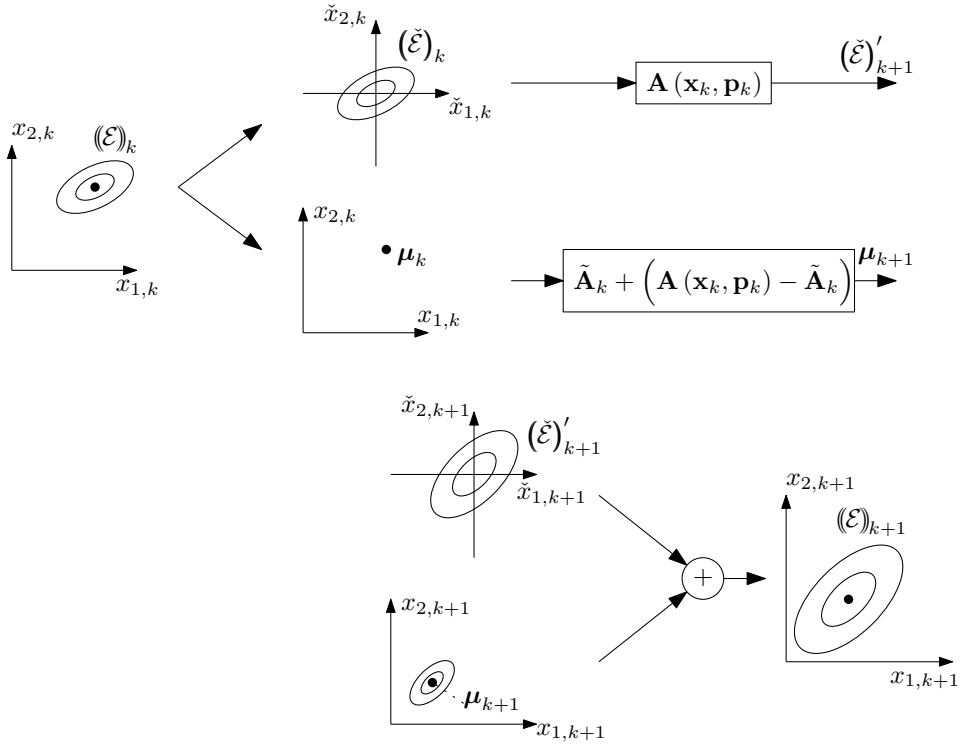

Figure 2: Separation of the state equations according to (15)–(19) into the mapping of an origin-centered ellipsoid and the verified treatment of non-zero offset terms.

1. Apply the mapping

$$\check{\mathbf{x}}_{k+1} = \mathbf{A}\left(\mathbf{x}_k, \mathbf{p}_k\right) \cdot \check{\mathbf{x}}_k \ , \tag{20}$$

with $\mathbf{A}\left(\mathbf{x}_k, \mathbf{p}_k\right)$ evaluated for all $\mathbf{x}_k \in \mathscr{E}_k^{\mathrm{O}}$ and $\mathbf{p}_k \in [\mathbf{p}_k]$, to the inner bound of $\left(\!\left(\check{\mathscr{E}}\right)\!\right)_k$ in (17). The shape matrix of the inner hull of the image set is given by

$$\check{\mathbf{Q}}_{k+1}^{\mathrm{I}} = \alpha_{\mathrm{I},k+1}^2 \cdot \underline{\rho}_k^2 \cdot \boldsymbol{\Gamma}_{k+1} \cdot \boldsymbol{\Gamma}_{k+1}^T \ , \tag{21}$$

where $\alpha_{\mathrm{I},k+1} \geq 0$ is the maximum value for which

$$\begin{aligned} \boldsymbol{\mathscr{N}}_{k+1} &:= \boldsymbol{\Lambda} \begin{bmatrix} \alpha_{\mathrm{I},k+1}^{-2} \cdot \boldsymbol{\mathscr{R}}_k^{-1} & \left(\tilde{\mathbf{A}}_k^{-1} \cdot \mathbf{A}\left(\mathbf{x}_k, \mathbf{p}_k\right)\right)^{-T} \\ \left(\tilde{\mathbf{A}}_k^{-1} \cdot \mathbf{A}\left(\mathbf{x}_k, \mathbf{p}_k\right)\right)^{-1} & \mathbf{Q}_k \end{bmatrix} \boldsymbol{\Lambda} \succeq 0 \ , \\ \mathbf{Q}_k &= \underline{\rho}_k^2 \cdot \boldsymbol{\Gamma}_k \cdot \boldsymbol{\Gamma}_k^T \end{aligned} \tag{22}$$

is satisfied in terms of positive semi-definiteness with the typical choice

$$\boldsymbol{\mathscr{R}}_k := \underline{\rho}_k^2 \cdot \boldsymbol{\Gamma}_k \cdot \boldsymbol{\Gamma}_k^T \ , \tag{23}$$

cf. [26]. An alternative choice for this matrix would be

$$\boldsymbol{\mathscr{R}}_k := \underline{\rho}_k^2 \cdot \tilde{\mathbf{A}}_k^{-T} \cdot \boldsymbol{\Gamma}_k \cdot \boldsymbol{\Gamma}_k^T \cdot \tilde{\mathbf{A}}_k^{-1} \ , \tag{24}$$

leading to a predicted ellipsoid that has an outer surface parallel to the one describing the state enclosure at the previous time step. As shown in [26], the option (24) is beneficial if the ratios of the lengths of the principal axes of the predicted ellipsoid differ significantly from the principal axes ratio of the original one. Note that the shape matrix definition (24) also simplifies the test for contractance in the following section.

As a generalization of the procedure derived in [26], the symmetric preconditioning matrix $\boldsymbol{\Lambda} = \boldsymbol{\Lambda}^T \succ 0$ is introduced in (22). It helps to optimize the ellipsoidal enclosures, especially for the propagation of small state domains, i.e., if the norms of $\left(\tilde{\mathbf{A}}_k^{-1} \cdot \mathbf{A}\left(\mathbf{x}_k, \mathbf{p}_k\right)\right)^{-T}$ and $\mathbf{Q}_k$ are significantly different. Then, the non-rescaled equation with $\boldsymbol{\Lambda} = \mathbf{I}$ may be too conservative and yield unnecessarily empty inner bounds[1]. For rescaling purposes, a block diagonal matrix $\boldsymbol{\Lambda} = \mathrm{blkdiag}\left(\beta\mathbf{I}, \beta^{-1}\mathbf{I}\right)$ with $\mathbf{I} \in \mathbb{R}^{n \times n}$ and the square root $\beta = \sqrt{\min\{\lambda_i\left(\mathbf{Q}_k\right)\}}$ of the smallest eigenvalue of $\mathbf{Q}_k$ is used in this paper.

2. Apply (20) to the outer bound of $\left(\!\left(\check{\mathscr{E}}\right)\!\right)_k$ in (17). The shape matrix of the outer hull of the image set is given by

$$\check{\mathbf{Q}}_{k+1}^{\mathrm{O}} = \alpha_{\mathrm{O},k+1}^2 \cdot \overline{\rho}_k^2 \cdot \boldsymbol{\Gamma}_{k+1} \cdot \boldsymbol{\Gamma}_{k+1}^T \ , \tag{25}$$

[1] Omitting this rescaling in the following computation of outer bounds may also turn the results unnecessarily wide and less useful when applied in the frame of proving stability.

where $\alpha_{\mathrm{O},k+1} \geq 0$ is the smallest value for which

$$\begin{aligned} \boldsymbol{\mathscr{M}}_{k+1} &:= \boldsymbol{\Lambda} \begin{bmatrix} -\mathbf{Q}_k^{-1} & \mathbf{A}^T(\mathbf{x}_k, \mathbf{p}_k) \cdot \tilde{\mathbf{A}}_k^{-T} \\ \tilde{\mathbf{A}}_k^{-1} \cdot \mathbf{A}(\mathbf{x}_k, \mathbf{p}_k) & -\alpha_{\mathrm{O},k+1}^2 \boldsymbol{\mathscr{R}}_k \end{bmatrix} \boldsymbol{\Lambda} \preceq 0 \ , \\ \mathbf{Q}_k &= \overline{\rho}_k^2 \cdot \boldsymbol{\Gamma}_k \cdot \boldsymbol{\Gamma}_k^T \end{aligned} \tag{26}$$

is satisfied for all $\mathbf{x}_k \in \mathscr{E}_k^{\mathrm{O}}$ and $\mathbf{p}_k \in [\mathbf{p}_k]$ with $\boldsymbol{\mathscr{R}}_k := \overline{\rho}_k^2 \cdot \boldsymbol{\Gamma}_k \cdot \boldsymbol{\Gamma}_k^T$.

3. Compute interval bounds for the term

$$\mathbf{b}_k = \left(\mathbf{A}(\mathbf{x}_k, \mathbf{p}_k) - \tilde{\mathbf{A}}_k \right) \cdot \boldsymbol{\mu}_k \in [\mathbf{b}_k] \tag{27}$$

which accounts for a non-zero ellipsoid midpoint with $\mathbf{x}_k$, $\tilde{\mathbf{A}}_k$, and $\mathbf{p}_k$ defined according to (16), (18), and (19). Deflate the inner ellipsoid bound from (21) according to

$$\mathbf{Q}_{k+1}^{\mathrm{I}} = \left(1 - \rho_{\mathrm{I},k+1}\right)^2 \cdot \check{\mathbf{Q}}_{k+1}^{\mathrm{I}} \ , \quad \rho_{\mathrm{I},k+1} = \sup \left\{ \left\| \alpha_{\mathrm{I},k+1}^{-1} \cdot \underline{\rho}_k^{-1} \cdot \boldsymbol{\Gamma}_k^{-1} \cdot [\mathbf{b}_k] \right\| \right\} \tag{28}$$

and inflate the outer bound in (25) with

$$\mathbf{Q}_{k+1}^{\mathrm{O}} = \left(1 + \rho_{\mathrm{O},k+1}\right)^2 \cdot \check{\mathbf{Q}}_{k+1}^{\mathrm{O}} \ , \quad \rho_{\mathrm{O},k+1} = \sup \left\{ \left\| \alpha_{\mathrm{O},k+1}^{-1} \cdot \overline{\rho}_k^{-1} \cdot \boldsymbol{\Gamma}_k^{-1} \cdot [\mathbf{b}_k] \right\| \right\} \ . \tag{29}$$

For $\rho_{\mathrm{I},k+1} \geq 1$, or if $\mathbf{A}(\mathbf{x}_k, \mathbf{p}_k)$ contains points at which it is not invertible, the inner bound becomes the empty set.

4. Compute the updated ellipsoid midpoint as

$$\boldsymbol{\mu}_{k+1} = \tilde{\mathbf{A}}_k \cdot \boldsymbol{\mu}_k \ . \tag{30}$$

5. The thick ellipsoid at the time instant $k+1$ then becomes

$$\mathbf{x}_{k+1} \in (\!(\mathscr{E})\!)_{k+1} \left(\boldsymbol{\mu}_{k+1}, \boldsymbol{\Gamma}_{k+1}, \left[\underline{\rho}_{k+1} \ ; \ \overline{\rho}_{k+1} \right] \right) \ , \tag{31}$$

where

$$\begin{aligned} \underline{\rho}_{k+1} &= \underline{\rho}_k \cdot \alpha_{\mathrm{I},k+1} \cdot \left(1 - \rho_{\mathrm{I},k+1}\right) \ , \\ \overline{\rho}_{k+1} &= \overline{\rho}_k \cdot \alpha_{\mathrm{O},k+1} \cdot \left(1 + \rho_{\mathrm{O},k+1}\right) \ , \quad \text{and} \\ \boldsymbol{\Gamma}_{k+1} &= \tilde{\mathbf{A}}_k \cdot \boldsymbol{\Gamma}_k \ . \end{aligned} \tag{32}$$

Remark 3. For eigenvalue tests according to [36] as well as a Gershgorin circle criterion [47] that both allow for checking the definiteness properties in (22) and (26), the reader is referred to [26].

3 Ellipsoidal Stability Contractor

3.1 Specification of the Initial State Domain

For what follows, we assume that a linearization of the system model (4) at the equilibrium point $\mathbf{x}_0 = \mathbf{0}$ is given by the Jacobian $\mathbf{J}_0 = \mathbf{J}(\mathbf{0})$, where

$$\mathbf{J}(\mathbf{x}) = \frac{\partial \mathbf{f}}{\partial \mathbf{x}}(\mathbf{x}) \quad . \tag{33}$$

For the quasi-linear model (14) with its equilibrium at the origin of the state space, $\mathbf{J}_0$ is chosen as

$$\mathbf{J}_0 = \mathbf{A}\left(\mathbf{0}, \mathrm{mid}\left([\mathbf{p}]\right)\right) \quad , \tag{34}$$

where $[\mathbf{p}]$ denotes an interval box containing all (temporally constant) uncertain system parameters.

3.1.1 Point-Valued Selection Approach

To find ellipsoidal domains as enclosures of the initial conditions, for which the likelihood of convergence to the equilibrium state is as large as possible, we do not purely assume axis-aligned initial state domains but rather exploit the local dynamics properties of the (linearized) system model.

In the simplest approach, a reasonable shape matrix for the initial ellipsoidal state domain can be determined by solving the discrete-time Lyapunov equation

$$\mathbf{J}_0^T \mathbf{P} \mathbf{J}_0 - \mathbf{P} = -\mathbf{I} \ . \tag{35}$$

Here, the actual choice of the matrix on the right-hand side represents a degree of freedom with the prerequisite to be negative definite (in (35), the negative identity matrix $-\mathbf{I}$ is used). To avoid specifying this matrix explicitly, the equality (35) can be cast equivalently into the LMI

$$\mathbf{J}_0^T \mathbf{P} \mathbf{J}_0 - \mathbf{P} \prec 0 \tag{36}$$

for which a solution $\mathbf{P} = \mathbf{P}^T \succ 0$ needs to be found. In analogy to a positive definite solution $\mathbf{P}$ of the Lyapunov equation (35), the existence of a solution to the LMI (36) corresponds to the local asymptotic stability of the linearized system model at the origin of the state space. The ellipsoid shape matrix $\mathbf{Q} = \mathbf{\Gamma} \cdot \mathbf{\Gamma}^T$ is then obtained according to the matrix inverse

$$\mathbf{Q} = \mathbf{P}^{-1} \ . \tag{37}$$

3.1.2 Robust Domain Specification

The drawback of the ellipsoid parameterization according to (35) and (36) is the fact that both approaches only take into account a point-valued system model in terms of a linearization at the equilibrium state. This restriction can be removed if

a polytopic uncertainty model is derived such that $\mathbf{J}(\mathbf{x})$ and $\mathbf{A}(\mathbf{x},\mathbf{p})$ with $\mathbf{p} \in [\mathbf{p}]$, respectively, are bounded by the convex polytopic domain

$$\mathbf{J}(\mathbf{x}) \in \left\{ \mathbf{J} \middle| \mathbf{J}(\xi) = \mathbf{J}'_0 + \sum_{v=1}^{n_v} \xi_v \cdot \Delta\mathbf{J}_v \ ; \quad \sum_{v=1}^{n_v} \xi_v = 1 \ ; \quad \xi_v \geq 0 \right\} \ . \tag{38}$$

Here, $\mathbf{x}$ needs to be replaced with a set-valued representation that encloses an application-motivated domain of interest for which stability shall be investigated. The domain (38) is spanned by a collection of at most $n_v = 2^{n^2}$ vertices, where the worst-case deviations of all possible realizations of the Jacobian $\mathbf{J}(\mathbf{x})$ from $\mathbf{J}'_0$ are described by the matrices $\Delta\mathbf{J}_v$. In (38), the matrix $\mathbf{J}'_0$ is a point-valued matrix included in the set-based evaluation of $\mathbf{J}(\mathbf{x})$, which is enclosed by a convex polytope that is spanned with the help of the individual increment matrices $\Delta\mathbf{J}_v$.

Using this formulation, (36) can be replaced in a conservative manner by the collection of LMIs

$$\left(\mathbf{J}'_0 + \Delta\mathbf{J}_v\right)^T \cdot \mathbf{P} \cdot \left(\mathbf{J}'_0 + \Delta\mathbf{J}_v\right) - \mathbf{P} \prec 0 \tag{39}$$

for which a joint solution $\mathbf{P} = \mathbf{P}^T \succ 0$ in terms of a vertex-independent quadratic Lyapunov function parameterization needs to be found. The existence of such a matrix $\mathbf{P}$ proves that each vertex realization, and hence all convex combinations of vertices according to (38), correspond to asymptotically stable realizations.

It should be pointed out that with the help of a quadratic Lyapunov function candidate $\mathbf{x}^T \cdot \mathbf{P} \cdot \mathbf{x}$ — that is parameterized according to (39) — only a proof of asymptotic stability for states satisfying the inequality

$$\mathbf{f}^T(\mathbf{x}_0) \cdot \mathbf{P} \cdot \mathbf{f}(\mathbf{x}_0) - \mathbf{x}_0^T \cdot \mathbf{P} \cdot \mathbf{x}_0 < 0 \tag{40}$$

in the interior of a contour line $\mathbf{x}_0^T \cdot \mathbf{P} \cdot \mathbf{x}_0 = c$, $c > 0$ that is fully included in the box $\mathbf{x}_0 \in [\mathbf{x}_0]$ is obtained. Note that this interval box needs to be employed for generating the polytopic uncertainty representation (38). Hence, the direct application of a stability contractor to the system models (4) and (14), making use of an ellipsoid with a shape matrix $\mathbf{Q}$ computed by (37) simplifies the evaluation of (40) and provides reasonably large provable stability domains as long as the contractor itself can be evaluated with a small amount of overestimation.

The major drawback of the polytopic uncertainty representation (38) is the typically large number of vertices that results from treating each matrix entry of the Jacobian (or of the quasi-linear system matrix, respectively) as independent.

Remark 4. The number n_v of the vertices to be considered in the polytopic uncertainty representation (38) can often be reduced by identifying physically motivated linear dependencies between individual entries of the matrix $\mathbf{J}(\mathbf{x})$ and by expressing them in terms of common interval parameters. For an example, where this has been done successfully, the reader is referred to [11].

When determining a candidate for the shape matrix of the initial state domain, in which stability is investigated, a further reduction of the complexity can be obtained by the introduction of a norm-bounded uncertainty model

$$\mathbf{J}\left(\mathbf{x}\right) \in \mathbf{J}_0 + \Delta\mathbf{J} \ , \quad \text{where} \quad \Delta\mathbf{J} = \mathbf{H} \cdot \mathbf{F} \cdot \mathbf{E} \tag{41}$$

holds with $\mathbf{F}$ being an unknown, norm-bounded matrix according to $\|\mathbf{F}\| < 1$. The example in Sec. 3.4 demonstrates how the matrices $\mathbf{E}$ and $\mathbf{H}$ included in (41) can be chosen to represent the variability of the matrix $\mathbf{J}\left(\mathbf{x}\right)$ over the investigated domain. There, the simplest choice is shown by setting one of the matrices to the identity matrix, and to define the second as the worst-case interval radii of each element of $\mathbf{J}\left(\mathbf{x}\right)$ if $\mathbf{J}_0$ is set to the element-wise defined interval midpoint. Using this norm-bounded model, a single LMI needs to be solved instead of finding a common solution to the previous list of n_v matrix inequalities.

Stability of the norm-bounded uncertainty model is verified according (39). Rewriting this inequality by applying the Schur complement formula leads to

$$\begin{bmatrix} -\mathbf{P} & \mathbf{J}_0^T \\ \mathbf{J}_0 & -\mathbf{P}^{-1} \end{bmatrix} + \begin{bmatrix} \mathbf{E}^T \\ \mathbf{0} \end{bmatrix} \mathbf{F}^T \begin{bmatrix} \mathbf{0} & \mathbf{H}^T \end{bmatrix} + \begin{bmatrix} \mathbf{0} \\ \mathbf{H} \end{bmatrix} \mathbf{F} \begin{bmatrix} \mathbf{E} & \mathbf{0} \end{bmatrix} \prec 0 \ , \quad \mathbf{P} \succ 0 \ . \tag{42}$$

Then, the application of the elimination lemma [40] allows for eliminating the unknown matrix $\mathbf{F}$. It turns the nonlinear matrix inequality[2] (42) into

$$\begin{bmatrix} -\mathbf{P} & \mathbf{J}_0^T \\ \mathbf{J}_0 & -\mathbf{P}^{-1} \end{bmatrix} + \epsilon^{-1} \begin{bmatrix} \mathbf{E}^T \\ \mathbf{0} \end{bmatrix} \begin{bmatrix} \mathbf{E} & \mathbf{0} \end{bmatrix} + \epsilon \begin{bmatrix} \mathbf{0} \\ \mathbf{H} \end{bmatrix} \begin{bmatrix} \mathbf{0} & \mathbf{H}^T \end{bmatrix} \prec 0 \ , \quad \mathbf{P} \succ 0 \ , \tag{43}$$

where $\epsilon > 0$ is a free parameter. After combining the second and third terms of the inequality (43), it becomes equivalent to

$$\begin{bmatrix} -\mathbf{P} & \mathbf{J}_0^T \\ \mathbf{J}_0 & -\mathbf{P}^{-1} \end{bmatrix} + \begin{bmatrix} \mathbf{E}^T \\ \epsilon\mathbf{H} \end{bmatrix} \epsilon^{-1}\mathbf{I} \begin{bmatrix} \mathbf{E} & \epsilon\mathbf{H}^T \end{bmatrix} \prec 0 \ , \quad \mathbf{P} \succ 0 \ , \tag{44}$$

which can be transformed by applying the Schur complement into

$$\begin{bmatrix} -\mathbf{P} & \mathbf{J}_0^T & \mathbf{E}^T \\ \mathbf{J}_0 & -\mathbf{P}^{-1} & \epsilon\mathbf{H} \\ \mathbf{E} & \epsilon\mathbf{H}^T & \epsilon\mathbf{I} \end{bmatrix} \prec 0 \ , \quad \mathbf{P} \succ 0 \ . \tag{45}$$

After multiplication of the matrix inequality (45) from the left and right with the block diagonal matrix

$$\text{blkdiag}\left(\mathbf{P}^{-1}, \mathbf{I}, \mathbf{I}\right) =: \text{blkdiag}\left(\mathbf{Q}, \mathbf{I}, \mathbf{I}\right) \ , \tag{46}$$

[2] due to the inverse of the decision variable matrix $\mathbf{P}$

the LMI formulation

$$\begin{bmatrix} -\mathbf{Q} & \mathbf{Q}\mathbf{J}_0^T & \mathbf{Q}\mathbf{E}^T \\ \mathbf{J}_0\mathbf{Q} & -\mathbf{Q} & \epsilon\mathbf{H} \\ \mathbf{E}\mathbf{Q} & \epsilon\mathbf{H}^T & \epsilon\mathbf{I} \end{bmatrix} \prec 0 \ , \quad \mathbf{Q} \succ 0 \tag{47}$$

is obtained. It verifies asymptotic stability of the norm-bounded uncertainty model (41) if $\mathbf{Q} = \mathbf{Q}^T \succ 0$ and, therefore, $\mathbf{P} = \mathbf{P}^T \succ 0$ exists, where the actual value of $\epsilon > 0$ can be determined automatically by the LMI solver.

3.2 Verification of the Property of Contractance

For the verification of the property of contractance in the case of a thick ellipsoid stability check, we assume that the prior state domain (given as a crisp ellipsoid $\mathscr{E}_0 = (\!(\mathscr{E})\!)_0 \left(\mathbf{0}, \mathbf{\Gamma}_0, [\rho_0 \ ; \ \rho_0]\right)$ with identical outer and inner bounds and a shape matrix parameterized according to the options listed in the previous subsection) is centered at the equilibrium state of the system (the origin, without loss of generality) and that it is mapped onto a thick ellipsoid $(\!(\mathscr{E})\!)_1 \left(\mathbf{0}, \mathbf{\Gamma}_1, \left[\underline{\rho}_1 \ ; \ \overline{\rho}_1\right]\right)$ that is again centered at the equilibrium.

Then, it is guaranteed by a one time step evaluation of the system model, that $\mathscr{E}_0$ belongs to the region of attraction of the equilibrium if the predicted outer bound $\mathscr{E}_1^{\mathrm{O}}$ is a guaranteed subset of $\mathscr{E}_0$ according to

$$\mathscr{E}_1^{\mathrm{O}} \subset \mathscr{E}_0 \ . \tag{48}$$

The property (48) can be checked by verifying whether *all* eigenvalues λ_i of the shape matrix difference satisfy the inequality[3]

$$\lambda_i = \lambda_i \left(\left(\overline{\rho}_1^2 \cdot \mathbf{\Gamma}_1 \cdot \mathbf{\Gamma}_1^T \right)^{-1} - \left(\rho_0^2 \cdot \mathbf{\Gamma}_0 \cdot \mathbf{\Gamma}_0^T \right)^{-1} \right) > 0 \ . \tag{49}$$

This inequality is a direct consequence of the proof of Theorem 3 in [26].

In contrast, if

$$\lambda_i = \lambda_i \left(\left(\underline{\rho}_1^2 \cdot \mathbf{\Gamma}_1 \cdot \mathbf{\Gamma}_1^T \right)^{-1} - \left(\rho_0^2 \cdot \mathbf{\Gamma}_0 \cdot \mathbf{\Gamma}_0^T \right)^{-1} \right) < 0 \tag{50}$$

holds for *all* of the eigenvalues according to the proof of Theorem 1 in [26], it is guaranteed that the domain $\mathscr{E}_0$ is an unstable neighborhood of the equilibrium $\mathbf{x}_0$ according to Chetaev's theorem, see [19, Theorem 3.12]. Geometrically, this

[3] A rigorous proof of the inequalities (49) and (50) is possible with the help of the routine `verifyeig` included in IntLab [39]. Alternatively, the matrices can be diagonalized as far as possible using verified numerics with a subsequent eigenvalue test following Remark 3. In many practical cases, however, it often suffices to check in classical floating point arithmetic whether the eigenvalues with smallest magnitude have a sufficiently large distance to the value zero.

corresponds to the fact that the predicted inner thick ellipsoid bound fully encloses the sufficiently small original domain according to

$$\mathscr{E}_1^{\mathrm{I}} \supset \mathscr{E}_0 \ . \tag{51}$$

Note, this case only arises for an intuitive choice of $\mathscr{E}_0$ (cf. Sec. 3.5) because it contradicts the robust LMI constraints listed above. Moreover, it should be noted that the difference $\overline{\rho}_1 - \underline{\rho}_1$ directly serves as a quantification of the possible overestimation of the predicted ellipsoid hulls according to [29].

The check of the eigenvalue inequalities (49) and (50) is necessary when applying either the general-purpose ellipsoidal enclosures according to Sec. 2.3 (Theorem 1) or when using the quasi-linear formulation (Sec. 2.4) with (23) as the parameterization for the predicted shape matrix. If the simplification (24) is used in the case of Sec. 2.4, the inequality (49) turns into $\overline{\rho}_1 < \rho_0$ and (50) turns into $\underline{\rho}_1 > \rho_0$.

To maximize the domains for which stability can be proven by this contractor, the examples in the following two subsections try to find the largest positive value ρ by means of a bisection algorithm so that $\min(\lambda_i) > 0$ holds in (49), where the threshold $\epsilon^* = 10^{-6}$ is used as the tolerance between two subsequent admissible solutions for the parameter ρ.

3.3 Proof of Stability: An Illustrating Example

As a first illustrating example, consider an explicit Euler discretization of the second-order system model $\dot{x}_1 = -x_1$, $\dot{x}_2 = -x_2 + x_1^2 x_2$ that was used in [15, 44] as a numerical benchmark scenario for the analysis of continuous-time ordinary differential equations. The discrete-time state equations can be specified as

$$\mathbf{x}_{k+1} = \mathbf{x}_k + T \cdot \begin{bmatrix} -x_{1,k} \\ -x_{2,k} + x_{1,k}^2 x_{2,k} \end{bmatrix} \quad \text{leading to} \quad \mathbf{J}_0 = \begin{bmatrix} 1-T & 0 \\ 0 & 1-T \end{bmatrix} \ , \tag{52}$$

which can be re-written (with the unique equilibrium $\mathbf{x}_0 = \mathbf{0}$) into the quasi-linear form

$$\mathbf{x}_{k+1} = \mathbf{A}(\mathbf{x}_k) \cdot \mathbf{x}_k = \begin{bmatrix} 1-T & 0 \\ T\alpha x_{1,k} x_{2,k} & (1-T) + T(1-\alpha) \cdot x_{1,k}^2 \end{bmatrix} \cdot \mathbf{x}_k \quad \text{with} \quad \alpha \in \mathbb{R} \ . \tag{53}$$

For this special example, $\mathbf{J}_0 = \mathbf{A}(\mathbf{0})$ holds. In general, the quasi-linear reformulation (53) is not unique. Therefore, the parameter α can be used as an optimization variable (in addition to the parameter ρ) of the initial ellipsoidal state domain in order to maximize the provable domain of attraction of the equilibrium.

Fig. 3 gives an overview of the provable stability domains by means of a symbolic evaluation of the discrete-time Lyapunov function increment (40) for a one time step evaluation of the system model. In Fig. 3, the result **A** denotes the maximum provable domain with the given Lyapunov function candidate; moreover, the general nonlinear ellipsoidal enclosure technique (result **B**), the quasi-linear ellipsoid

implementation (result **C**) as well as an interval-based contractor implementation (result **D**) are compared. Due to the fact that the system model has a dominant linear behavior in the close vicinity to the equilibrium, the quasi-linear evaluation outperforms the general nonlinear technique. Moreover, it can be seen that the actual choice of the parameter α has a strong influence on the volume of the provable stability domain, where the maximum-volume ellipsoid is close to the volume of the largest provable box volume in the case of Figs. 3a and 3b and even larger for the heuristic choice of Figs. 3c and 3d. Note that the visible spikes in the volume dependency can be removed by slightly adapting the scaling matrix $\mathbf{\Lambda}$ in (26).

Due to the fact that all domains shown in the left column of Fig. 3 are guaranteed to contain asymptotically stable system realizations, their set-valued union can be formed to describe the domain in the state space for which the system exhibits asymptotically stable dynamics. The fact that the quasi-linear contractor outperforms the general nonlinear ellipsoidal enclosures gives rise to the following aspect of future work: Find a unified implementation for both approaches in which the quasi-linear system matrix and/or a suitable interval extension in slope arithmetic [6, 38] are employed to enhance the tightness of solutions. Note that the interval contractor was evaluated in an overestimation-free manner for this example after a symbolic reformulation of the state equations. This fact emphasizes the advantageous property of the ellipsoidal approach in Figs. 3a and 3c to prove stability of initial conditions that could not be detected by the interval counterpart for the same choice of aspect ratio (resulting from the precomputed ellipsoid shape matrix $\mathbf{Q}$).

In Figs. 3e and 3f, however, it can be seen that the ellipsoid enclosures are much smaller than the interval contractor's volume. This is caused by the fact that the included matrices $\mathbf{J}(\mathbf{x})$ need to be evaluated on a box that encloses the ellipsoid domain from the outside which leads to a kind of wrapping effect. For this specific setting of the shape matrix $\mathbf{Q}$, parts of those domains are close to the stability boundary so that the ellipsoid approach performs worse than the interval-based counterpart. In such cases, the approaches included in [13, 14] for the computation of outer state enclosures could be helpful to enhance the procedures of [3]. In general, however, the ellipsoidal approach will be more efficient if the domains under investigation are chosen on the basis of Lyapunov function candidates.

3.4 Stability Proof of an EKF-Based Localization Algorithm

As a second application scenario, we re-consider the stability proof of an EKF-based localization algorithm, for which an interval-based stability contractor was investigated in [3].

For this scenario, the output equation is given by

$$\mathbf{y}_k = \mathbf{h}(\mathbf{x}_k) = \begin{bmatrix} (x_{1,k} - a_1)^2 + (x_{2,k} - a_2)^2 \\ (x_{1,k} - b_1)^2 + (x_{2,k} - b_2)^2 \end{bmatrix} \quad , \tag{54}$$

where (a_1, a_2) and (b_1, b_2) denote the known positions of two beacons; the vector $\mathbf{y}_k$ denotes the squared distances to the object $\mathbf{x}_k$ to be localized. This measurement

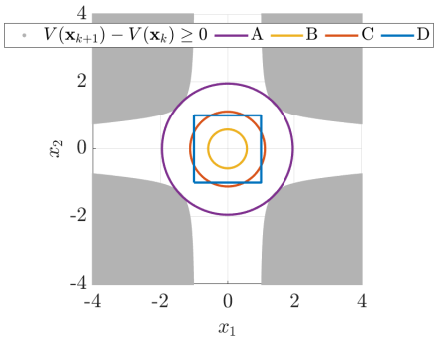

(a) Selection of $\mathbf{P} = \mathbf{Q}^{-1}$ acc. to (35), (36).

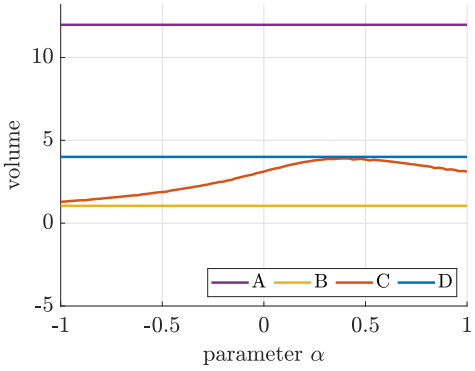

(b) Selection of $\mathbf{P} = \mathbf{Q}^{-1}$ acc. to (35), (36).

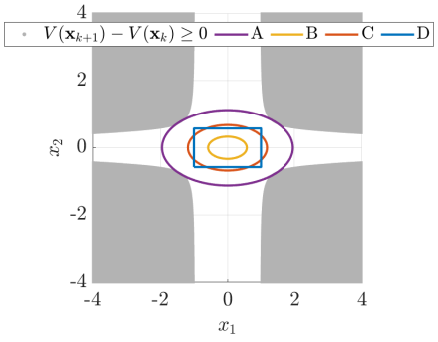

(c) Selection of $\mathbf{P} = \mathbf{Q}^{-1} = \mathrm{diag}\left([1 \quad 3]\right)$.

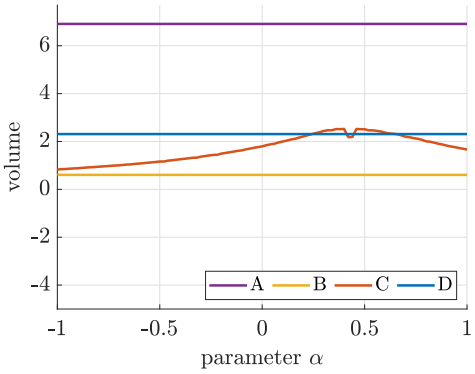

(d) Selection of $\mathbf{P} = \mathbf{Q}^{-1} = \mathrm{diag}\left([1 \quad 3]\right)$.

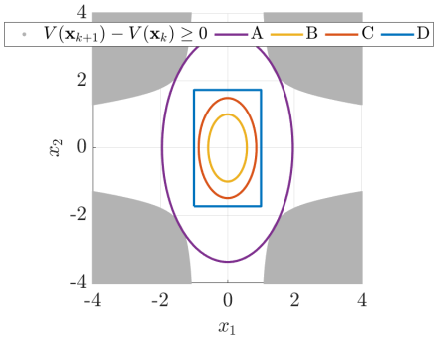

(e) Selection of $\mathbf{P} = \mathbf{Q}^{-1} = \mathrm{diag}\left([3 \quad 1]\right)$.

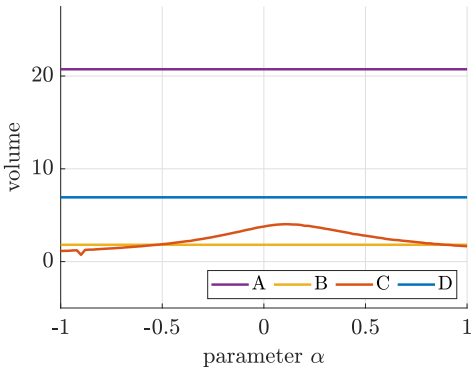

(f) Selection of $\mathbf{P} = \mathbf{Q}^{-1} = \mathrm{diag}\left([3 \quad 1]\right)$.

Figure 3: Provable stability domains for the example (52), (53) in the left column (using the parameter α with the largest ellipsoid volume in the case **C**) and dependence of the volume of the provable stability domain on the parameter $\alpha \in [-1\ ;\ 1]$ (right column).

(subscript m) is assumed to be corrupted by additive, zero-mean Gaussian noise $\mathbf{v}_k$ with the covariance $\mathbf{C}_v$, so that $\mathbf{y}_{\mathrm{m},k} = \mathbf{y}_k + \mathbf{v}_k$ holds. Moreover, we assume that the object to be localized is described by a discrete-time integrator disturbance model with additive, zero-mean Gaussian process noise $\mathbf{w}_k$ according to

$$\begin{bmatrix} x_{1,k+1} \\ x_{2,k+1} \end{bmatrix} = \begin{bmatrix} x_{1,k} \\ x_{2,k} \end{bmatrix} + \mathbf{w}_k \ , \tag{55}$$

where the disturbance covariance matrix related to $\mathbf{w}_k$ is denoted by $\mathbf{C}_w$.

Then, an EKF algorithm can be specified with the help of the augmented state vector

$$\mathbf{x}_k = \begin{bmatrix} x_{1,k} & x_{2,k} & c_{11,k} & c_{12,k} & c_{22,k} \end{bmatrix}^T \ , \tag{56}$$

which consists of the estimated position $(x_{1,k}, x_{2,k})$ and the entries of the covariance matrix $\mathbf{C}_k$ after the innovation stage at the time instant k. The position and covariance matrix can be extracted with the help of selection matrices

$$\mathbf{S}_1 = \begin{bmatrix} 1 & 0 & 0 & 0 & 0 \\ 0 & 1 & 0 & 0 & 0 \end{bmatrix} \quad \text{and} \quad \mathbf{S}_2 = \begin{bmatrix} 0 & 0 & 1 & 0 & 0 \\ 0 & 0 & 0 & 1 & 0 \\ 0 & 0 & 0 & 0 & 1 \end{bmatrix} \ , \tag{57}$$

where

$$\begin{bmatrix} x_{1,k} \\ x_{2,k} \end{bmatrix} = \mathbf{S}_1 \cdot \mathbf{x}_k \tag{58}$$

and

$$\begin{bmatrix} c_{11,k} \\ c_{12,k} \\ c_{22,k} \end{bmatrix} = \mathrm{vech}\left(\mathbf{C}_k\right) = \mathbf{S}_2 \cdot \mathbf{x}_k \ , \ \ \mathbf{C}_k = \begin{bmatrix} c_{11,k} & c_{12,k} \\ c_{12,k} & c_{22,k} \end{bmatrix} \iff \mathbf{C}_k = \mathrm{vech}^{-1}\left(\mathbf{S}_2 \cdot \mathbf{x}_k\right) \ . \tag{59}$$

Here, extracting the upper triangular part of the covariance matrix $\mathbf{C}_k$ is performed by the half-vectorization operator vech, where the corresponding inverse operation is denoted by vech^{-1}. With this notation, the state equations of the EKF can be specified so that $\mathbf{x}_{k+1}$ contains the estimated position and covariance matrix entries after performing the subsequent prediction and innovation step associated with the time instant $k+1$. Hence, these equations are given by

$$\mathbf{x}_{k+1} = \mathbf{f}\left(\mathbf{x}_k\right) = \begin{bmatrix} \mathbf{S}_1 \cdot \mathbf{x}_k + \mathbf{K}\left(\mathbf{x}_k\right) \cdot \left(\mathbf{y}_{\mathrm{m},k} - \mathbf{h}\left(\mathbf{x}_k\right)\right) \\ \mathrm{vech}\left(\left(\mathbf{I} - \mathbf{K}\left(\mathbf{x}_k\right) \cdot \mathbf{H}\left(\mathbf{x}_k\right)\right) \cdot \mathbf{C}_{k+1}^{\mathrm{p}}\left(\mathbf{x}_k\right)\right) \end{bmatrix} \tag{60}$$

with the predicted covariance matrix

$$\mathbf{C}_{k+1}^{\mathrm{p}}\left(\mathbf{x}_k\right) = \mathrm{vech}^{-1}\left(\mathbf{S}_2 \cdot \mathbf{x}_k\right) + \mathbf{C}_w \ , \tag{61}$$

the Kalman gain

$$\mathbf{K}\left(\mathbf{x}_k\right) = \mathbf{C}_{k+1}^{\mathrm{p}}\left(\mathbf{x}_k\right) \cdot \mathbf{H}^T\left(\mathbf{x}_k\right) \cdot \left(\mathbf{H}\left(\mathbf{x}_k\right) \cdot \mathbf{C}_{k+1}^{\mathrm{p}}\left(\mathbf{x}_k\right) \cdot \mathbf{H}^T\left(\mathbf{x}_k\right) + \mathbf{C}_v\right)^{-1} \ , \tag{62}$$

and the Jacobian

$$\mathbf{H}\left(\mathbf{x}_k\right) = \left[\frac{\partial \mathbf{h}}{\partial x_{1,k}}\left(\mathbf{x}_k\right) \quad \frac{\partial \mathbf{h}}{\partial x_{2,k}}\left(\mathbf{x}_k\right)\right] \tag{63}$$

of the output equation with respect to the current position estimate. For the following numerical results in Tabs. 1 and 2, we consider the beacon positions $a_1 = -5$, $a_2 = 5$, $b_1 = 5$, $b_2 = 5$, the measurement $\mathbf{y}_{\mathrm{m},k} = \begin{bmatrix}0 & 0\end{bmatrix}^T$, and the noise covariances $\mathbf{C}_w = \mathrm{diag}\left(\begin{bmatrix}0.01 & 0.01\end{bmatrix}\right)$ as well as $\mathbf{C}_v = \mathrm{diag}\left(\begin{bmatrix}1 & 1\end{bmatrix}\right)$. This leads to the equilibrium state $x_1^* = x_2^* = 0$, $c_{12}^* = 0$ and $c_{11}^* = c_{22}^* = 0.003660254037844$ around which the stability domains are centered.

Using a point-valued selection of the ellipsoid shape matrix according to Sec. 3.1.1 leads to the result in Tab. 1 which can be widened by the robustified, norm-bounded uncertainty representation according to Sec. 3.1.2, see Tab. 2. For that purpose, the norm-bounded uncertainty model in (41) is parameterized by choosing $\mathbf{E} = \mathbf{I}$. Then, the matrix $\mathbf{H}$ is specified so that the maximum interval radii of an interval extension of the Jacobian $\mathbf{J}\left(\mathbf{x}\right)$ on a representative domain are captured in an element-wise sense by the additive term $\Delta\mathbf{J}$. It should be pointed out that the provably stable interval box domains are significantly larger than those reported in [3]. This is caused (*i*) by choosing the ratios of the interval edge lengths identical to the ratios of the edge lengths of an axis-aligned box corresponding to the Lyapunov function and LMI-based shape matrix definitions, and (*ii*) by not only using a centered form evaluation but also intersecting it with a slope extension of the range implemented in IntLab [38, 39]. This kind of evaluation can also be integrated into the ellipsoidal approach in future work.

3.5 Proof of Instability: An Illustrating Example

To demonstrate the applicability of the ellipsoidal approach to find unstable neighborhoods of equilibrium points by means of (51) and the inequality (50), consider the explicit Euler discretization with $T = 0.1$ of the benchmark example (3.23) in [19] for which $\beta = 1$ is chosen. In a quasi-linear form, this example has the state equations

$$\mathbf{x}_{k+1} = \left(\mathbf{I} + T \cdot \begin{bmatrix}\beta^2 - x_{1,k}^2 - x_{2,k}^2 & 1 \\ -1 & \beta^2 - x_{1,k}^2 - x_{2,k}^2\end{bmatrix}\right) \cdot \mathbf{x}_k \ . \tag{64}$$

Parameterizing the initial state domain $\mathscr{E}_0$ as a circle with radius 0.1 leads to circles as the inner ellipsoidal enclosures $\mathscr{E}_1^{\mathrm{I}}$ with the inward rounded radii 0.10953174 and 0.11002215 for the general-purpose and the quasi-linear evaluation approaches of Secs. 2.3 and 2.4, respectively. Due to $\mathscr{E}_1^{\mathrm{I}} \supset \mathscr{E}_0$, the domain $\mathscr{E}_0$ is a provably unstable neighborhood of the equilibrium $\mathbf{x}_0 = \mathbf{0}$, where the quasi-linear approach provides the less conservative solution.

Table 1: Comparison of different stability contractors for a shape matrix selection according to Sec. 3.1.1; for the ellipsoid case, a tight outer, axis-aligned hull is given.

	interval contractor	
	$\underline{\mathbf{x}}$	$\overline{\mathbf{x}}$
x_1	−0.00427481791343	0.00427481791343
x_2	−0.00427481599897	0.00427481599897
c_{11}	−0.00076536378418	0.00808587185987
c_{12}	−0.00442561782520	0.00442561782520
c_{22}	−0.00076536379689	0.00808587187258

	ellipsoidal encl. (quasi-lin.)	
	$\underline{\mathbf{x}}$	$\overline{\mathbf{x}}$
x_1	−0.00161026895377	0.00161026895377
x_2	−0.00161026823262	0.00161026823262
c_{11}	0.00199318069709	0.00532732737860
c_{12}	−0.00166707334195	0.00166707334195
c_{22}	0.00199318069230	0.00532732738339

	ellipsoidal encl. (general.)	
	$\underline{\mathbf{x}}$	$\overline{\mathbf{x}}$
x_1	−0.00043890766400	0.00043890766400
x_2	−0.00043890746744	0.00043890746744
c_{11}	0.00320586332007	0.00411464475562
c_{12}	−0.00045439071810	0.00045439071810
c_{22}	0.00320586331877	0.00411464475692

Table 2: Comparison of different stability contractors for a robustified shape matrix selection according to Sec. 3.1.2; for the ellipsoid case, a tight outer, axis-aligned hull is given.

	interval contractor	
	$\underline{\mathbf{x}}$	$\overline{\mathbf{x}}$
x_1	−0.00440136214825	0.00440136214825
x_2	−0.00440079183131	0.00440079183131
c_{11}	−0.00076807607385	0.00808858414954
c_{12}	−0.00441865927874	0.00441865927874
c_{22}	−0.00076814256179	0.00808865063748

	ellipsoidal encl. (quasi-lin.)	
	$\underline{\mathbf{x}}$	$\overline{\mathbf{x}}$
x_1	−0.00168345510722	0.00168345510722
x_2	−0.00168323696953	0.00168323696953
c_{11}	0.00196648408848	0.00535402398721
c_{12}	−0.00169007100059	0.00169007100059
c_{22}	0.00199318069230	0.00535404941785

	ellipsoidal encl. (general.)	
	$\underline{\mathbf{x}}$	$\overline{\mathbf{x}}$
x_1	−0.00044551035825	0.00044551035825
x_2	−0.00044545263019	0.00044545263019
c_{11}	0.00321201395487	0.00410849412082
c_{12}	−0.00044726119141	0.00044726119141
c_{22}	0.00321200722490	0.00410850085079

4 Outlook: Ellipsoid Definition of Positive Invariant Sets for Continuous-Time Processes

Due to the fact that the ellipsoidal contractor above is based on a forward in time evaluation of dynamic system models, it is also readily applicable to the continuous-time case if the solution approach published in [27] is employed. However, to reduce pessimism, it can be combined in future work with the following novel test for positive invariance.

Theorem 2 (Positive invariant, ellipsoidal domains for continuous-time systems)**.** *Consider the continuous-time system* $\dot{\mathbf{x}}(t) = \mathbf{f}\left(\mathbf{x}(t)\right)$, $\mathbf{x} \in \mathbb{R}^n$ *with the (locally) stable equilibrium* $\mathbf{x} = \mathbf{0}$. *Define the Lyapunov function candidate*

$$V\left(\mathbf{x}(t)\right) = \frac{1}{2}\mathbf{x}^T \boldsymbol{\mathscr{P}} \mathbf{x} \ , \quad \mathbf{x} := \mathbf{x}(t) \tag{65}$$

with $\boldsymbol{\mathscr{P}} \succ 0$ *and the small interval box* $[\mathbf{x}] \ni \mathbf{0}$. *Define the ellipsoid*

$$\mathscr{E}_{\boldsymbol{\mathscr{P}}}\left([\mathbf{x}]\right) = \left\{ \mathbf{x} \in \mathbb{R}^n \ \middle| \ -\mathbf{x}^T \cdot \boldsymbol{\mathscr{P}} \cdot \frac{\partial \mathbf{f}}{\partial \mathbf{x}}\left(\mathbf{0}\right) \cdot \mathbf{x} \leq v^+ \right\} \tag{66}$$

with

$$v^+ = \sup\left([\mathbf{x}]^T \cdot \boldsymbol{\mathscr{P}} \cdot [\mathbf{e}] \right) \quad \textit{and} \quad [e_i] = \frac{1}{2}\,[\mathbf{x}]^T \cdot \frac{\partial^2 f_i}{\partial \mathbf{x}^2}\left([\mathbf{x}]\right) \cdot [\mathbf{x}] \ . \tag{67}$$

If $\mathscr{E}_{\boldsymbol{\mathscr{P}}}\left([\mathbf{x}]\right) \subset [\mathbf{x}]$, $\mathscr{E}_{\boldsymbol{\mathscr{P}}}\left([\mathbf{x}]\right)$ *is positive invariant.*

Proof. Take an interval box $\mathbf{x}$ with center at $\mathbf{x} = \mathbf{0}$ and express the i-th component of $\mathbf{f}$ as a second-order Taylor form near the equilibrium, i.e.,

$$\mathbf{x} \in [\mathbf{x}] \Longrightarrow f_i\left(\mathbf{x}\right) \in J_{i:} \cdot \mathbf{x} + \frac{1}{2}\,[\mathbf{x}]^T \cdot [\mathbf{H}_i] \cdot [\mathbf{x}] = J_{i:} \cdot \mathbf{x} + [e_i] \ , \tag{68}$$

where $[\mathbf{H}_i]$ is an interval extension of the Hessian of f_i and $J_{i:}$ is the i-th row of the Jacobian $\mathbf{J} = \frac{\partial \mathbf{f}}{\partial \mathbf{x}}\left(\mathbf{0}\right)$. Consequently,

$$\begin{aligned} \dot{V}\left(\mathbf{x}\right) &= \mathbf{x}^T \cdot \boldsymbol{\mathscr{P}} \cdot \mathbf{f}\left(\mathbf{x}\right) \\ &= \sum_{i=1}^{n} x_i \cdot \mathscr{P}_{:i} \cdot f_i\left(\mathbf{x}\right) \\ &\in \sum_{i=1}^{n} x_i \cdot \mathscr{P}_{:i} \cdot \left(J_{i:} \cdot \mathbf{x} + [e_i]\right) \\ &= \mathbf{x}^T \cdot \boldsymbol{\mathscr{P}} \cdot \mathbf{J} \cdot \mathbf{x} + \mathbf{x}^T \cdot \boldsymbol{\mathscr{P}} \cdot [\mathbf{e}] \ . \end{aligned} \tag{69}$$

Setting $[v] = [\mathbf{x}]^T \cdot \boldsymbol{\mathscr{P}} \cdot [\mathbf{e}]$, we have $\dot{V}\left(\mathbf{x}\right) < \mathbf{x}^T \cdot \boldsymbol{\mathscr{P}} \cdot \mathbf{J} \cdot \mathbf{x} + \sup\left([v]\right)$. Taking $\mathbf{x}$ such that $\mathbf{x}^T \cdot \boldsymbol{\mathscr{P}} \cdot \mathbf{J} \cdot \mathbf{x} + v^+ = 0$, where $v^+ \sup\left([v]\right)$, yields $\dot{V}\left(\mathbf{x}\right) < 0$ for $\mathbf{x} \in \mathscr{E}_{\boldsymbol{\mathscr{P}}}\left([\mathbf{x}]\right)$ according to (66), (67) which completes the proof. □

5 Conclusions

In this paper, an ellipsoidal implementation of a stability contractor was presented for discrete-time systems. Due to the possibility for finding initial parameterizations of the shape matrix by means of Lyapunov equations or LMIs, it has the advantage in comparison to a straightforward interval-based implementation that the considered domains are not necessarily axis-parallel and that the form of the domains investigated is close to (locally valid) Lyapunov function candidates. In such a way, it becomes possible to often find larger domains of attraction than for the previously investigated interval-based counterpart. In addition, it was shown that the use of a specialized implementation for quasi-linear system models may outperform the application of a general ellipsoidal enclosure technique. This is especially true if free parameters in the quasi-linear system models are used as further degrees of freedom to optimize the volume of the provable stability domain.

In future work, the approach will not only be used for a stability analysis of dynamic systems but also to optimize controllers so that the domains of attraction of stable operating points become as large as possible. Moreover, it is reasonable to consider not only set-valued uncertainty representations, but also links to techniques which simultaneously allow for robustifying control procedures in the presence of stochastic noise [11, 28, 32]. Finally, applications to continuous-time processes, in combination with the new invariance test sketched in Sec. 4, will be investigated.

References

[1] Althoff, M. and Rath, J. Comparison of guaranteed state estimators for linear time-invariant systems. *Automatica*, 130:109662, 2021. DOI: `10.1016/j.automatica.2021.109662`.

[2] Barmish, B.R. *New Tools for Robustness of Linear Systems*. Macmillan, New York, 1994.

[3] Bourgois, A. *Safe & Collaborative Autonomous Underwater Docking*. PhD thesis, ENSTA Bretagne, Brest, France, 2021.

[4] Bourgois, A. and Jaulin, L. Interval centred form for proving stability of non-linear discrete-time systems. In Dang, Thao and Ratschan, Stefan, editors, *Proceedings 6th International Workshop on Symbolic-Numeric methods for Reasoning about CPS and IoT*, volume 331 of *Electronic Proceedings in Theoretical Computer Science*, pages 1–17. Open Publishing Association, 2021. DOI: `10.4204/EPTCS.331.1`.

[5] Boyd, S., El Ghaoui, L., Feron, E., and Balakrishnan, V. *Linear Matrix Inequalities in System and Control Theory*. SIAM, Philadelphia, 1994. DOI: `10.1137/1.9781611970777`.

[6] Chapoutot, A. Interval slopes as a numerical abstract domain for floating-point variables. *Lecture Notes in Computer Science*, pages 184—200, 2010. DOI: 10.1007/978-3-642-15769-1_12.

[7] Chesi, G. On the estimation of the domain of attraction for uncertain polynomial systems via LMIs. In *43rd IEEE Conference on Decision and Control*, volume 1, pages 881–886, 2004. DOI: 10.1109/CDC.2004.1428796.

[8] Chesi, G. Robust static output feedback controllers via robust stabilizability functions. *IEEE Transactions on Automatic Control*, 59(6):1618–1623, 2014. DOI: 10.1109/TAC.2013.2293453.

[9] Chilali, M. and Gahinet, P. H_∞ design with pole placement constraints: An LMI approach. *IEEE Transactions on Automatic Control*, 41(3):358–367, 1996. DOI: 10.1109/9.486637.

[10] Cornelius, H. and Lohner, R. Computing the range of values of real functions with accuracy higher than second order. *Computing*, 33:331–347, 1984. DOI: 10.1007/BF02242276.

[11] Dehnert, R., Damaszek, M., Lerch, S., Rauh, A., and Tibken, B. Robust feedback control for discrete-time systems based on iterative LMIs with polytopic uncertainty representations subject to stochastic noise. *Frontiers in Control Engineering*, 2, 2022. DOI: 10.3389/fcteg.2021.786152.

[12] Delanoue, N., Jaulin, L., and Cottenceau, B. An algorithm for computing a neighborhood included in the attraction domain of an asymptotically stable point. *Communications in Nonlinear Science and Numerical Simulation*, 21(1):181–189, 2015. DOI: 10.1016/j.cnsns.2014.08.034.

[13] Goubault, E. and Putot, S. Robust under-approximations and application to reachability of non-linear control systems with disturbances. *IEEE Control Systems Letters*, 4(4):928–933, 2020. DOI: 10.1109/LCSYS.2020.2997261.

[14] Goubault, E. and Putot, S. Tractable higher-order under-approximating AE extensions for non-linear systems. In *Proceedings of the 7th IFAC Conference on Analysis and Design of Hybrid Systems*, 2021. DOI: 10.1016/j.ifacol.2021.08.504.

[15] Hachicho, O. and Tibken, B. Estimating domains of attraction of a class of nonlinear dynamical systems with LMI methods based on the theory of moments. In *Proceedings of the 41st IEEE Conference on Decision and Control*, volume 3, pages 3150–3155, 2002. DOI: 10.1109/CDC.2002.1184354.

[16] Jaulin, L., Kieffer, M., Didrit, O., and Walter, É. *Applied Interval Analysis*. Springer–Verlag, London, 2001. DOI: 10.1007/978-1-4471-0249-6.

[17] Kersten, J., Rauh, A., and Aschemann, H. Interval methods for robust gain scheduling controllers: An LMI-based approach. *Granular Computing*, pages 203–216, 2020. DOI: 10.1007/s41066-018-00147-1.

[18] Khalil, H.K. *Nonlinear Systems*. Prentice-Hall, Upper Saddle River, New Jersey, 3rd edition, 2002.

[19] Marquez, H.J. *Nonlinear Control Systems*. John Wiley & Sons, Inc., New Jersey, 2003.

[20] Mayer, G. *Interval Analysis and Automatic Result Verification*. De Gruyter Studies in Mathematics. De Gruyter, Berlin/Boston, 2017. DOI: 10.1515/9783110499469.

[21] Merlet, J.-P. Interval analysis for certified numerical solution of problems in robotics. *International Journal of Applied Mathematics and Computer Science*, 19(3):399–412, 2009. DOI: 10.2478/v10006-009-0033-3.

[22] Monfared, M.N. and Yazdanpanah, M.J. Optimal dynamic Lyapunov function and the largest estimation of domain of attraction. *IFAC-PapersOnLine, Proceedings of the 20th IFAC World Congress*, 50(1):2645–2650, 2017. DOI: 10.1016/j.ifacol.2017.08.469.

[23] Nedialkov, N.S. Interval tools for ODEs and DAEs. In *CD-Proceedings of the 12th GAMM-IMACS International Symposium on Scientific Computing, Computer Arithmetic, and Validated Numerics*, Duisburg, Germany, 2007. IEEE Computer Society. DOI: 10.1109/SCAN.2006.28.

[24] Pepy, R., Kieffer, M., and Walter, E. Reliable robust path planning with application to mobile robots. *International Journal of Applied Mathematics and Computer Science*, 19(3):413–424, 2009. DOI: 10.2478/v10006-009-0034-2.

[25] Pursche, T., Swiatlak, R., and Tibken, B. Estimation of the domain of attraction for nonlinear autonomous systems using a Bezoutian approach. In *SICE International Symposium on Control Systems*, pages 1–6, 2016. DOI: 10.1109/SICEISCS.2016.7470159.

[26] Rauh, A., Bourgois, A., and Jaulin, L. Union and intersection operators for thick ellipsoid state enclosures: Application to bounded-error discrete-time state observer design. *Algorithms*, 14(3):88, 2021. DOI: 10.3390/a14030088.

[27] Rauh, A., Bourgois, A., Jaulin, L., and Kersten, J. Ellipsoidal enclosure techniques for a verified simulation of initial value problems for ordinary differential equations. In *Proceedings of the 5th International Conference on Control, Automation and Diagnosis (ICCAD'21)*, Grenoble, France, 2021. DOI: 10.1109/ICCAD52417.2021.9638755.

[28] Rauh, A., Dehnert, R., Romig, S., Lerch, S., and Tibken, B. Iterative solution of linear matrix inequalities for the combined control and observer design of systems with polytopic parameter uncertainty and stochastic noise. *Algorithms*, 14:205, 2021. DOI: 10.3390/a14070205.

[29] Rauh, A. and Jaulin, L. A computationally inexpensive algorithm for determining outer and inner enclosures of nonlinear mappings of ellipsoidal domains. *International Journal of Applied Mathematics and Computer Science*, 31(3):399–415, 2021. DOI: 10.34768/amcs-2021-0027.

[30] Rauh, A. and Jaulin, L. A novel thick ellipsoid approach for verified outer and inner state enclosures of discrete-time dynamic systems. In *Proceedings of the 19th IFAC Symposium System Identification: Learning Models for Decision and Control*, Padova, Italy (online), 2021. DOI: 10.1016/j.ifacol.2021.08.426.

[31] Rauh, A., Kersten, J., and Aschemann, H. Toward the optimal parameterization of interval-based variable-structure state estimation procedures. *Reliable Computing*, 25:118–132, 2017. www.cs.utep.edu/interval-comp/reliable-computing-25-pp-118-132.pdf.

[32] Rauh, A. and Romig, S. Linear matrix inequalities for an iterative solution of robust output feedback control of systems with bounded and stochastic uncertainty. *Sensors*, 21(9):3285, 2021. DOI: 10.3390/s21093285.

[33] Rauh, A., Senkel, L., and Aschemann, H. Interval-based sliding mode control design for solid oxide fuel cells with state and actuator constraints. *IEEE Transactions on Industrial Electronics*, 62(8):5208–5217, 2015. DOI: 10.1109/TIE.2015.2404811.

[34] Rauh, A., Senkel, L., and Aschemann, H. Reliable sliding mode approaches for the temperature control of solid oxide fuel cells with input and input rate constraints. In *Proceedings of the 1st IFAC Conference on Modelling, Identification and Control of Nonlinear Systems*, St. Petersburg, Russia, 2015. DOI: 10.1016/j.ifacol.2015.09.217.

[35] Rauh, A., Senkel, L., Kersten, J., and Aschemann, H. Reliable control of high-temperature fuel cell systems using interval-based sliding mode techniques. *IMA Journal of Mathematical Control and Information*, 33:457–484, 2016. DOI: 10.1093/imamci/dnu051.

[36] Rohn, J. Positive definiteness and stability of interval matrices. *SIAM Journal on Matrix Analysis and Applications*, 15(1):175–184, 1994. DOI: 10.1137/S0895479891219216.

[37] Romig, S., Jaulin, L., and Rauh, A. Using interval analysis to compute the invariant set of a nonlinear closed-loop control system. *Algorithms*, 12(12):262, 2019. DOI: 10.3390/a12120262.

[38] Rump, S.M. Expansion and estimation of the range of nonlinear functions. *Mathematics of Computation*, 65(216):1503–1512, 1996. DOI: 10.1090/S0025-5718-96-00773-9.

[39] Rump, S.M. IntLab — INTerval LABoratory. In Csendes, T., editor, *Developments in Reliable Computing*, pages 77–104. Kluver Academic Publishers, 1999. DOI: 10.1007/978-94-017-1247-7_7.

[40] Scherer, C. and Weiland, S. Linear matrix inequalities in control. In Levine, W.S., editor, *Control System Advanced Methods*, The Electrical Engineering Handbook Series, pages 24–1—24–30. CRC Press, Boca Raton, 2nd edition, 2011. DOI: 10.1201/b10384.

[41] Skelton, R.E. Linear matrix inequality techniques in optimal control. In Baillieul, John and Samad, Tariq, editors, *Encyclopedia of Systems and Control*, pages 1–10. Springer London, London, 2020. DOI: 10.1007/978-1-4471-5102-9_207-2.

[42] Stengel, R. *Optimal Control and Estimation*. Dover Publications, Inc., New York, USA, 1994.

[43] Swiatlak, R., Tibken, B., Paradowski, T., and Dehnert, R. Determination of the optimal quadratic Lyapunov function for nonlinear autonomous systems via interval arithmetic. In *European Control Conference (ECC)*, pages 297–303, 2015. DOI: 10.1109/ECC.2015.7330560.

[44] Tibken, B. Estimation of the domain of attraction for polynomial systems via LMIs. In *Proceedings of the 39th IEEE Conference on Decision and Control*, volume 4, pages 3860–3864, 2000. DOI: 10.1109/CDC.2000.912314.

[45] Tibken, B. and Hachicho, O. Estimation of the domain of attraction for polynomial systems using multidimensional grids. In *Proceedings of the 39th IEEE Conference on Decision and Control*, volume 4, pages 3870–3874, 2000. DOI: 10.1109/CDC.2000.912316.

[46] Valmórbida, G., Tarbouriech, S., and Garcia, G. Region of attraction estimates for polynomial systems. In *Proceedings of the 48h IEEE Conference on Decision and Control (CDC) held jointly with 2009 28th Chinese Control Conference*, pages 5947–5952, 2009. DOI: 10.1109/CDC.2009.5399969.

[47] Weinmann, A. *Uncertain Models and Robust Control*. Springer–Verlag, Wien, 1991. DOI: 10.1007/978-3-7091-6711-3.

Received 26th August 2021